Electronic Supplementary Material (ESI) for Journal of Materials Chemistry A.

Ultralow thermal conductivity in the mixed-anion solid solution $Sn_2SbS_{2-x}Se_xI_3$

Justin Mark,[a,#] Wenhao Zhang,[a,b,#] Kazuhiko Maeda,[c] Takafumi Yamamoto,[d] Hiroshi Kageyama[e] and Takao Mori[a,b,*]

[a] *International Center for Materials Nanoarchitectonics (WPI-MANA), National Institute for Materials Science (NIMS), Tsukuba, Ibaraki 305-0044, Japan*
[b] *Graduate School of Pure and Applied Science, University of Tsukuba, Tsukuba, Ibaraki 305-8671, Japan*
[c] *Department of Chemistry, School of Science, Tokyo Institute of Technology, Tokyo, Japan*
[d] *Laboratory for Materials and Structures, Tokyo Institute of Technology, Yokohama, Japan*
[e] *Graduate School of Engineering, Kyoto University, Kyoto, Japan*

[#] J.M. and W.Z. contributed equally to this work

[*] Corresponding author, e-mail: MORI.takao@nims.go.jp

Supporting Information

PPMS Correction for additional radiation loss

Correcting radiation loss with larger emissivity

PPMS TTO measures the thermal conductivity by measuring sample thermal conductance. The sample thermal conductance is given by:

$$K = \left(I^2R - P_{rad}/\Delta T\right) - K_{shoe}$$

where I^2R is the heater power provided at one end of the sample. P_{rad} is the power lost through radiation. ΔT is the temperature difference and K_{shoe} is the thermal conductance of the shoe.

Radiation loss is estimated by:

$$P_{rad} = \frac{S}{2}\sigma_T\varepsilon\left(T_{hot}^{\ 4} - T_{cold}^{\ 4}\right)$$

The T^4 terms give the strong dependence of radiation loss with temperature, S is the sample's surface area, σ_T is the Stefan-Boltzmann constant and ε is the infrared emissivity.

According to the TTO manual, for metallic surfaces, $\varepsilon \approx 0.3$ and for nonmetallic surfaces, $\varepsilon \approx 1.0$. During our measurement, we used an $\varepsilon = 0.5$ as measurement parameter. But for our sample, it is more appropriate to use the values near $\varepsilon \approx 1.0$.

We therefore apply additional correction after the measurement by increasing the sample emissivity. In the raw datafile of PPMS TTO, I^2R, ΔT and P_{rad} are all recorded. Since P_{rad} is linear in ε, we multiply P_{rad} by 2.0, corresponding to $\varepsilon = 1.0$ and then recalculate the thermal conductance and finally, the thermal conductivity is given by:

$$\kappa = Kl/A$$

where A is the cross-section area of the sample and l is the length between the temperature measurement.

Analysis of error in the thermal conductivity measurement

The error in the laser flash measurement comes from the error in determining C_p and the error in estimating the thermal diffusivity, the combined error is under 10%, according to the instrument manual.

The error in PPMS TTO measurement is much larger. In our measurement, the error in the measurement at 300 K is about ± 0.12 W/mK. Furthermore, the error in the estimation of radiation loss can be up to 1mW/K (thermal conductance), as described in the manual. With our non-optimal sample geometry ($L \approx 3.3mm$ and $A \approx 4.6mm^2$ with L and A is the distance between two contact and the cross-section area), this translates to an error in thermal conductivity as large as 0.72 W/mK. In conclusion, large systematic error in thermal conductivity measured above 150 K can be expected. However, our main observation that a board peak in thermal conductivity at low temperature is present is not affected by the errors at higher temperature.

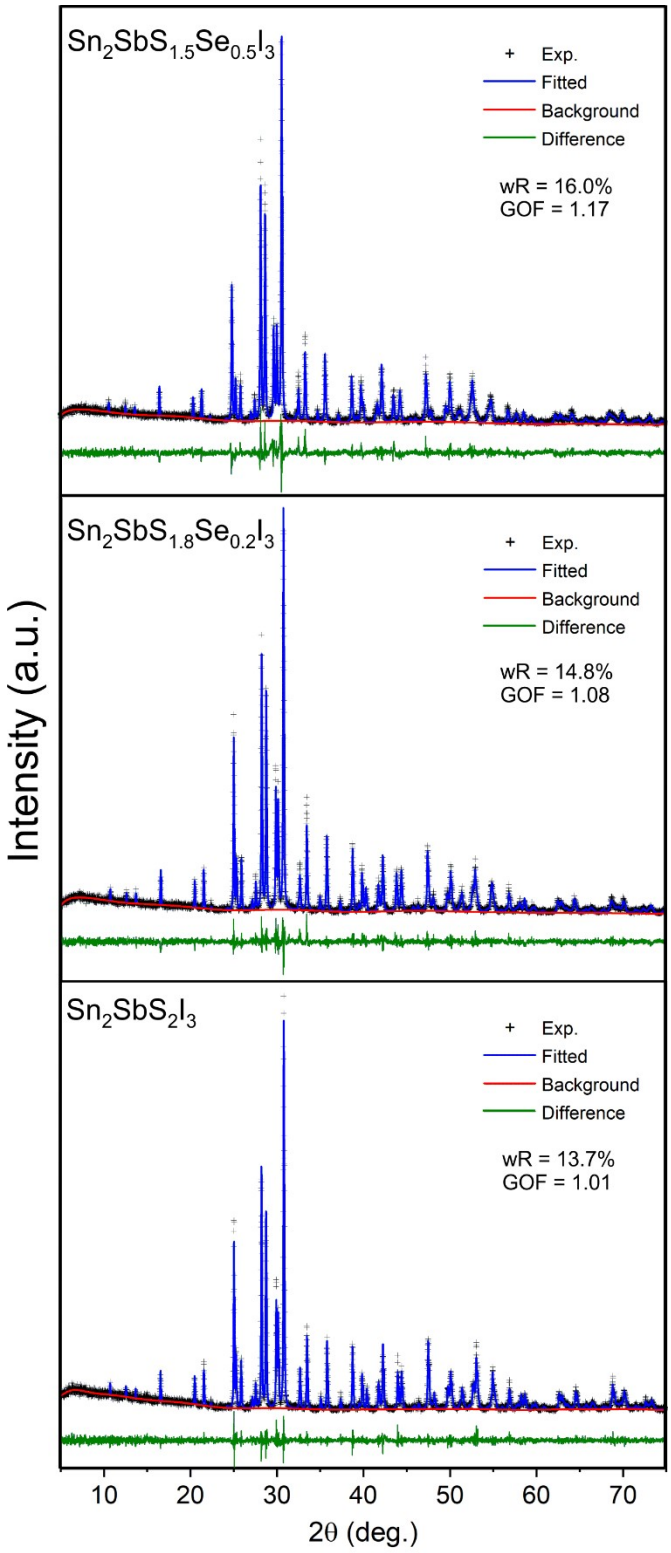

Figure S1. Rietveld refinement for $Sn_2SbS_{2-x}Se_xI_3$ (x = 0, 0.2, 0.5) samples fit to the reported $Sn_2SbS_2I_3$ structure.[1]

Table S1. Lattice parameters of $Sn_2SbS_{2-x}Se_xI_3$ determined through Rietveld refinement compared to reported single crystal unit cells of $Sn_2SbS_2I_3$ and $Sn_2SbSe_2I_3$.[1]

	[1]Reported $Sn_2SbS_2I_3$	$Sn_2SbS_2I_3$	$Sn_2SbS_{1.8}Se_{0.2}I_3$	$Sn_2SbS_{1.5}Se_{0.5}I_3$	[1]Reported $Sn_2SbSe_2I_3$
a (Å)	4.275(1)	4.272(1)	4.278(2)	4.284(1)	4.298(3)
b (Å)	14.059(3)	14.067(4)	14.077(4)	14.084(3)	14.085(5)
c (Å)	16.465(3)	16.456(4)	16.519(6)	16.627(4)	17.222(8)

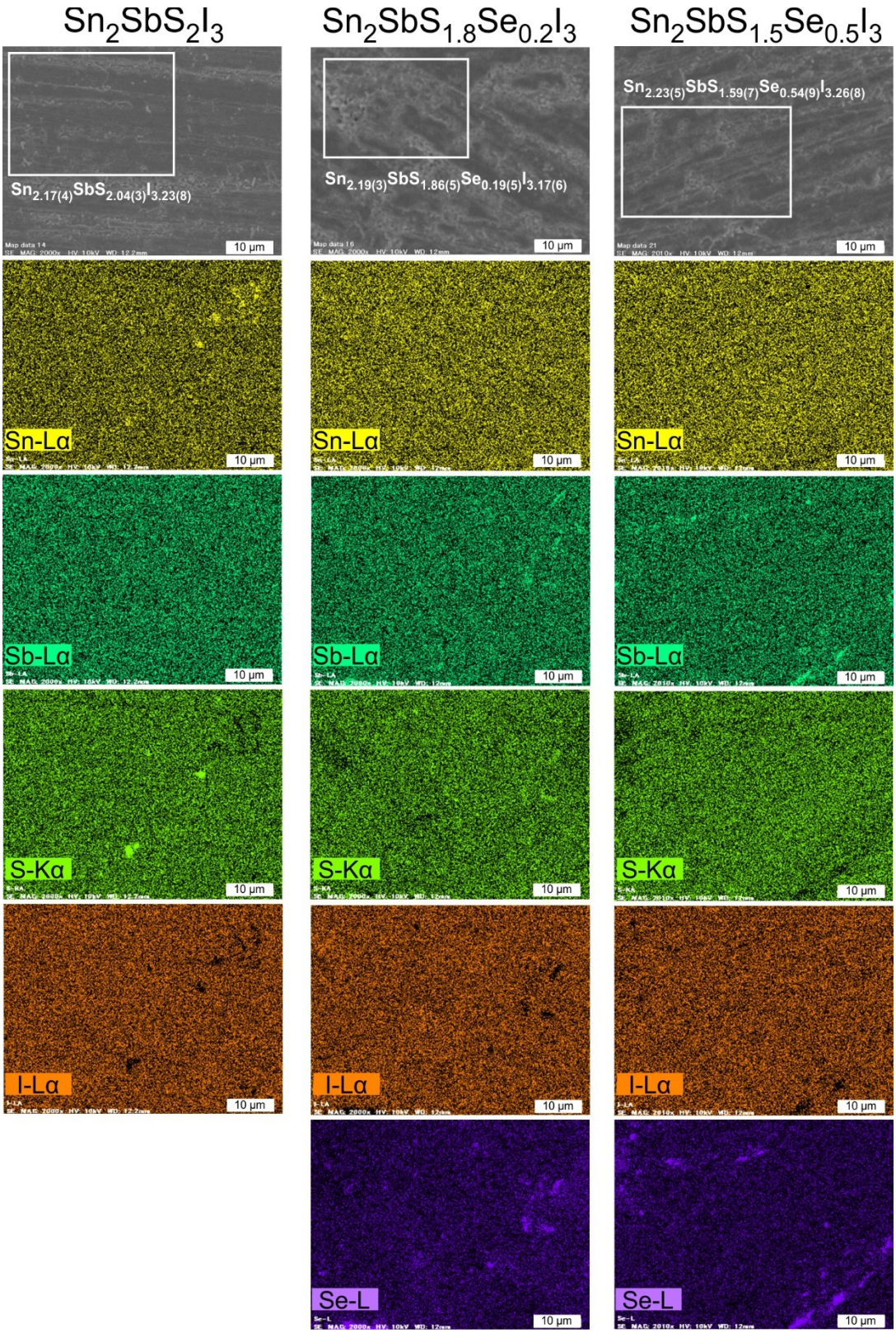

Figure S2. SEM-EDS images of $Sn_2SbS_{2-x}Se_xI_3$ (x = 0, 0.2, 0.5). Areas used for bulk composition determination are highlighted by white boxes and labeled with the respective determined compositions.

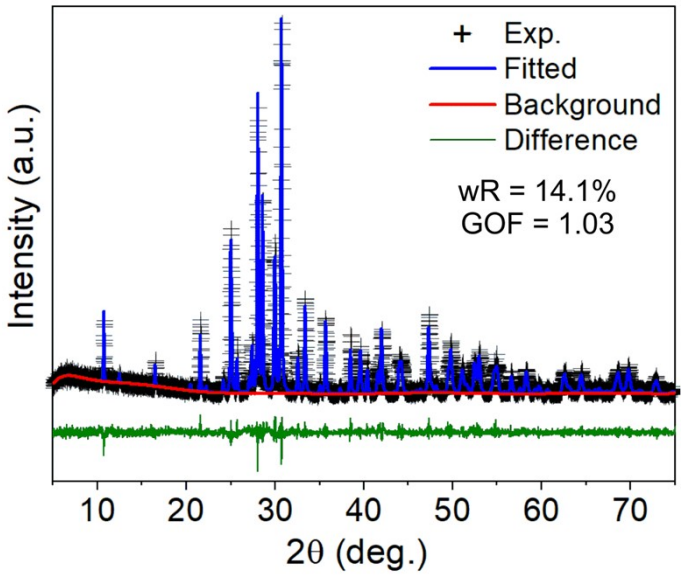

Figure S3. Rietveld refinement for synthesized $Sn_2BiS_2I_3$ sample fit to the reported $Sn_2BiS_2I_3$ structure.[2]

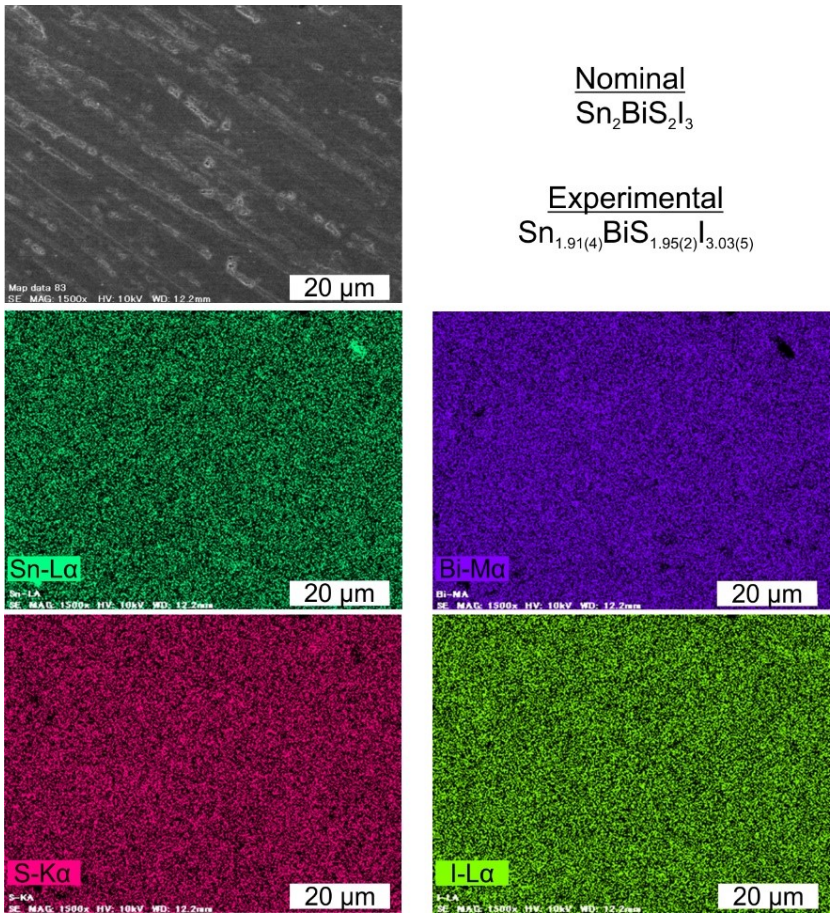

Figure S4. SEM-EDS images of $Sn_2BiS_2I_3$. Experimental composition is normalized to 1 Bi and is an average of three measured spots.

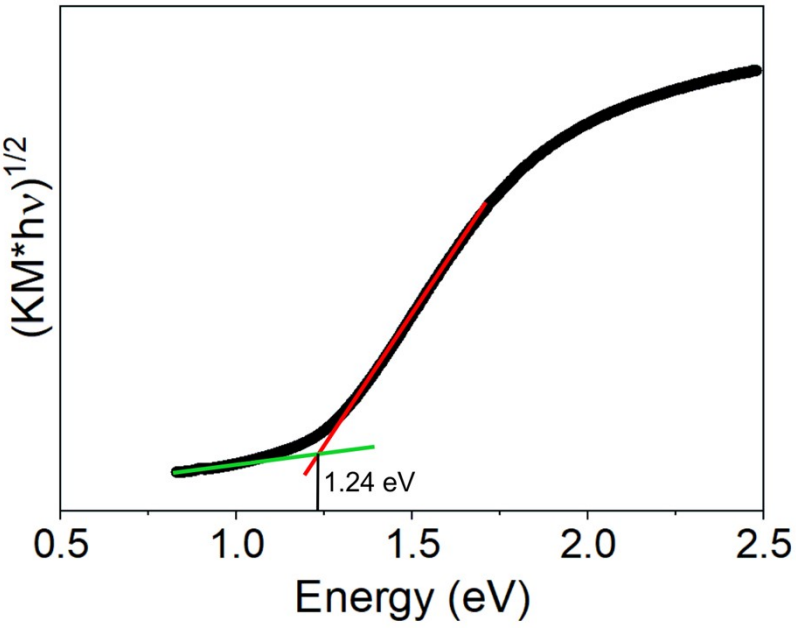

Figure S5. Indirect bandgap Tauc plot of solid state UV-Vis Kubelka-Munk diffuse reflectance spectra for $Sn_2BiS_2I_3$.

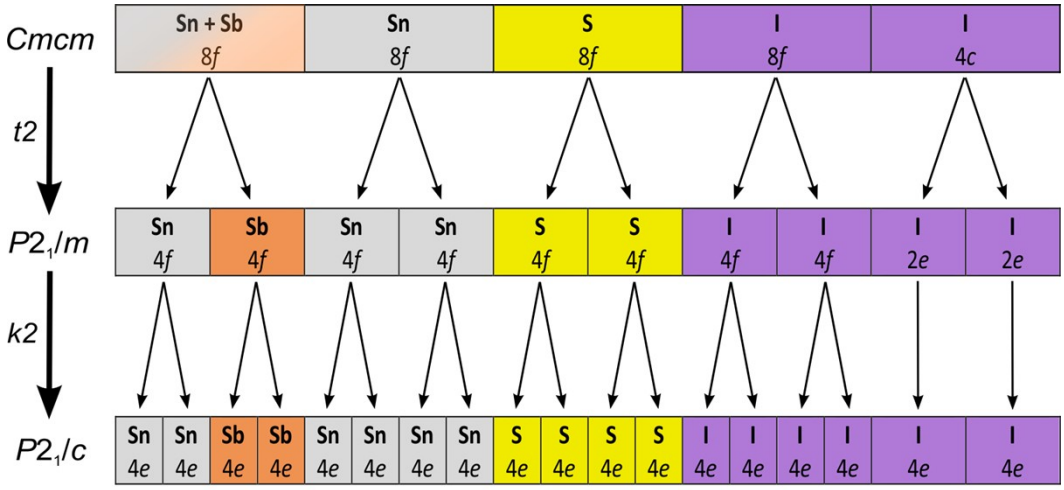

Figure S6. Group-subgroup relationship of $Sn_2SbS_2I_3$ *Cmcm* and $P2_1/c$ structures illustrating the splitting of the Wyckoff positions.

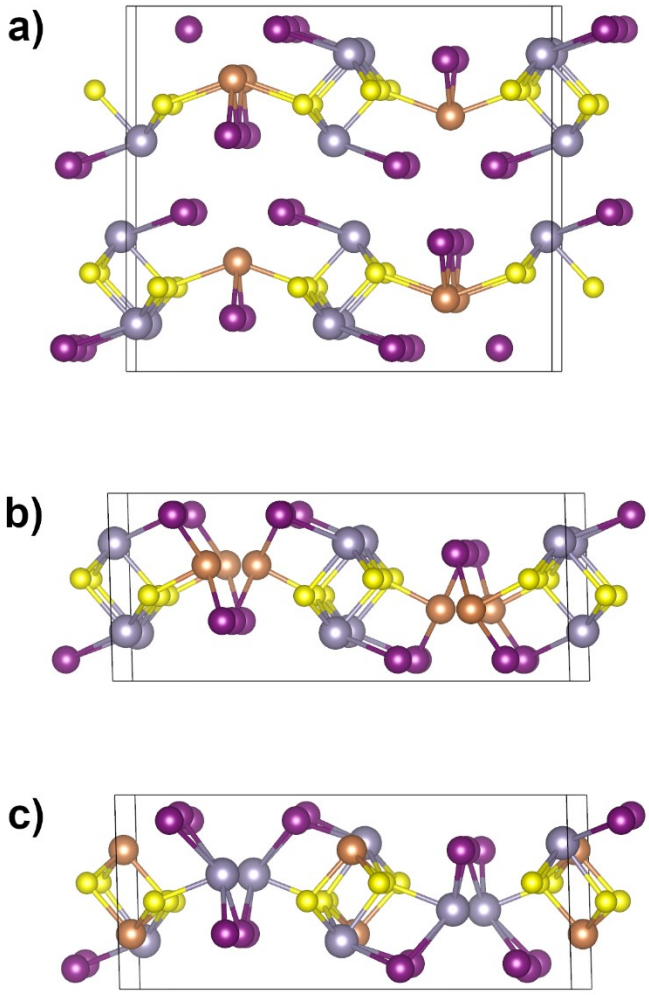

Figure S7. $Sn_2SbS_2I_3$ structures a) *Cmcm*-4*c*, b) $P2_1/c$ -(*Cmcm*) and c) LT-$P2_1/c$ considered for computational analysis. The colors correspond to the colors used in the article: gray: Sn, orange: Sb, yellow: S and purple: I. Notice how the Sb atom displace away from *Cmcm*-4*c* to $P2_1/c$ -(*Cmcm*), and the Sn and Sb atom change position in LT-$P2_1/c$.

Table S2. The lattice parameter of the DFT relaxed structure models, corresponding to $Cmcm$-4c, $P2_1/c$ -(*Cmcm*) and LT-$P2_1/c$ structures

	$Cmcm$-4c	$P2_1/c$-$Cmcm$	LT-$P2_1/c$
a	4.275	7.441	7.472
b	14.059	17.350	16.744
c	16.365	8.627	8.616
α	90	90	90
β	90	107.418	106.65
γ	90	90	90
Sn	$4a$ (0.000,0.147,0.529)	$4e$ (0.257,0.477,0.292)	$4e$ (0.590,0.227,0.157)
Sn	$4a$ (0.000,0.109,0.984)	$4e$ (0.266,0.017,0.336)	$4e$ (0.248,0.480,0.307)
Sb	$4a$ (0.000,0.214,0.277)	$4e$ (0.617,0.206,0.135)	$4e$ (0.283,0.014,0.325)
S	$4a$ (0.000,0.286,0.416)	$4e$ (0.454,0.419,0.116)	$4e$ (0.454,0.415,0.098)
S	$4a$ (0.000,0.253,0.084)	$4e$ (0.457,0.079,0.109)	$4e$ (0.451,0.076,0.126)
I	$4a$ (0.000,0.575,0.355)	$4e$ (0.115,0.624,0.028)	$4e$ (0.106,0.621,0.031)
I	$4a$ (0.000,0.541,0.117)	$4e$ (0.320,0.250,0.332)	$4e$ (0.285,0.256,0.326)
I	$4a$ (0.000,0.137,0.743)	$4e$ (0.115,0.640,0.524)	$4e$ (0.131,0.621,0.531)

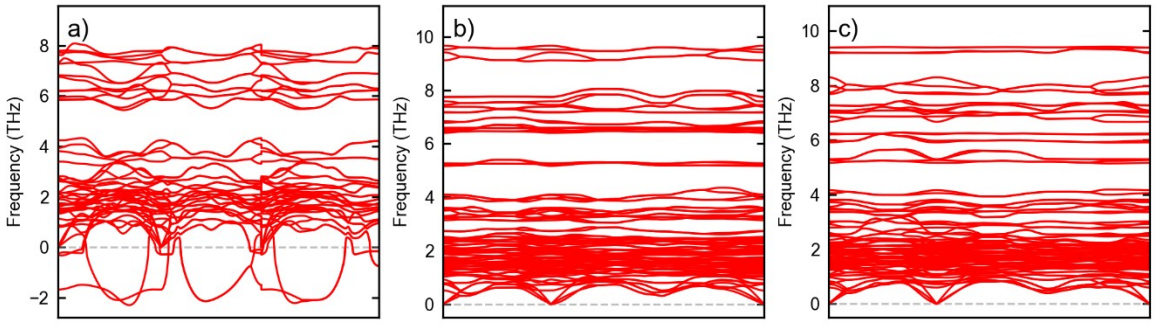

Figure S8. Calculated phonon dispersion of a) *Cmcm*-4c, b) $P2_1/c$ -(*Cmcm*) and c) LT-$P2_1/c$ structures of $Sn_2SbS_2I_3$.

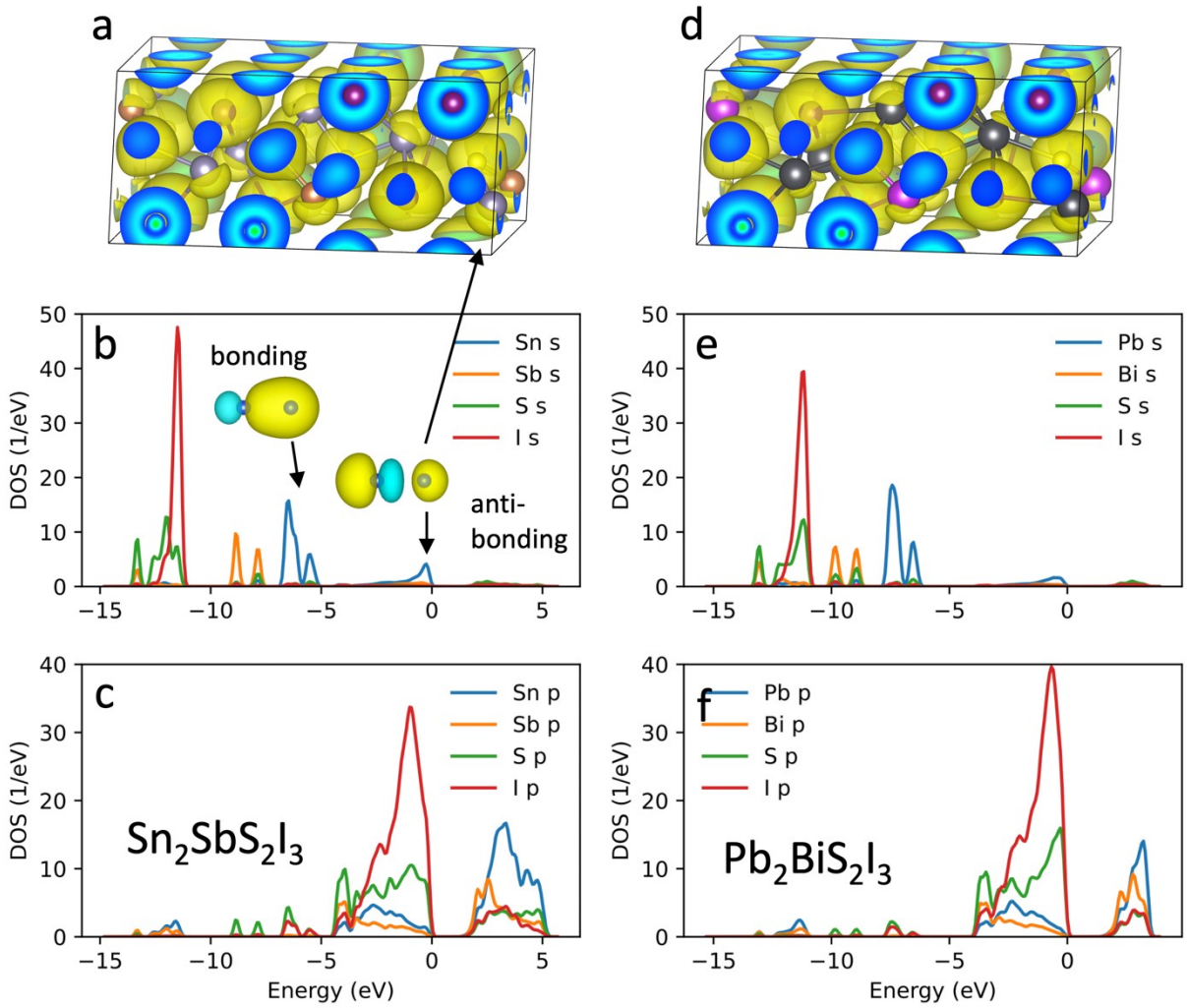

Figure S9. Confirmation of the assignment of electron localized region to the s orbitals of Pb and Sb near the top of the valence band. a) the integrated local density of states for $Sn_2SbS_2I_3$. b) the projected density of states of $Sn_2SbS_2I_3$ showing the s orbital component of Sn. The inset shows a simplified picture of bonding states related to Sn s orbital. c) the projected density of states of $Sn_2SbS_2I_3$ for the p orbitals. d)—f), the same figures but for $Pb_2BiS_2I_3$, which does not show a strong anti-bonding s state from Pb near the valence band maximum corresponding density in the anti-bonding region in real space. Note that this 'crescent moon' shaped electron density overlaps with the same shape in ELF plot (Figure 6)

References

1. Ibanez, A.; Jumas, J.-C.; Olivier-Fourcade, J.; Philippot, E., Mise en evidence d'un desordre statistique dans les structures chalcogenoiodures d'etain et d'antimoine. *J. Solid State Chem.* **1984,** *55*, 83-91.

2. Islam, S. M.; Malliakas, C. D.; Sarma, D.; Maloney, D. C.; Stoumpos, C. C.; Kontsevoi, O. Y.; Freeman, A. J.; Kanatzidis, M. G., Direct Gap Semiconductors $Pb_2BiS_2I_3$, $Sn_2BiS_2I_3$, and Sn_2BiSI_5. *Chem. Mater.* **2016,** *28*, 7332-7343.